Modeling Disordered Morphologies in Organic Semiconductors

Tobias Neumann,[a,b] Denis Danilov,[b] Christian Lennartz,[c] and Wolfgang Wenzel*[a,b]

Organic thin film devices are investigated for many diverse applications, including light emitting diodes, organic photovoltaic and organic field effect transistors. Modeling of their properties on the basis of their detailed molecular structure requires generation of representative morphologies, many of which are amorphous. Because time-scales for the formation of the molecular structure are slow, we have developed a linear-scaling single molecule deposition protocol which generates morphologies by simulation of vapor deposition of molecular films. We have applied this protocol to systems comprising argon, buckminsterfullerene, N,N-Di(naphthalene-1-yl)-N,N'-diphenyl-benzidine, mertris (8-hydroxy-quinoline)aluminum(III), and phenyl-C_{61}-butyric acid methyl ester, with and without postdeposition relaxation of the individually deposited molecules. The proposed single mole-cule deposition protocol leads to formation of highly ordered morphologies in argon and buckminsterfullerene systems when postdeposition relaxation is used to locally anneal the configura-tion in the vicinity of the newly deposited molecule. The other systems formed disordered amorphous morphologies and the postdeposition local relaxation step has only a small effect on the characteristics of the disordered morphology in comparison to the materials forming crystals.

Introduction

Optoelectronic devices based on organic materials may have unique electrical and optical properties, regarding quantum/power efficiency or emission/absorption properties, which may combine with the advantage of low cost manufacture processing.[1,2] Organic light emitting diodes (OLEDs), for example, typically have a layered structure and can be fabricated sequentially by vapor deposition or solution processing of organic charge-transport and emitter materials. The prevalent morphology of the material layers is an amorphous film of either small molecules or polymers.[1–3] The disorder in the morphology and a weak electronic coupling between the molecules lead to states described by quantum-mechanical wave functions that are essentially localized on single molecules.[4,5] Because of this localization, charge transport takes place by hopping of charge carriers from one molecule to another and the hopping probabilities depending strongly on the overlap between molecular orbitals on adjacent sites.[4,5] As a consequence, the charge transport properties of organic semiconductors are extremely sensitive to the morphology of the material.[6–8]

A crucial quantity describing the quality of the organic semiconductors is the mobility of the charge carriers, which is defined as the average velocity of the charge carriers divided by the electric field that causes their motion.[5] The mobility in single-crystal materials can reach the values of order of several $cm^2/(V\,s)$ at room temperature. In disordered films, the mobility of the charge carriers is orders of magnitude lower than those of crystalline materials.[6] Nevertheless, practical applications of thin-film organic semiconductors often rely on disordered materials to manufacture large-scale and flexible devices. The strong influence of the morphology on key properties of organic semiconductors (i.e., the mobility of the charge carriers) calls for the development of efficient simulation approaches to generate sufficiently large disordered morphologies to permit predictive modeling and optimization of the properties of organic materials.

There are different approaches to model the solid-state morphology of thin organic films. A common method to simulate amorphous morphologies is the molecular dynamics (MD) approach,[9–12] but the simulation time is typically much shorter than deposition times in experiment. MD simulations often attempt to circumvent this problem by heating the system above the melting temperature.[9–12] After the equilibration at high temperature, the system is rapidly cooled down to the target temperature, which may be below the glass temperature for the system in question. Simulations in the nanosecond range correspond to a very high cooling rate, which might result in trapping the amorphous structure in a local minimum of the energy landscape. A different approach to simulate the morphology of organic films is based on Monte Carlo (MC) methods.[13] In this case, larger individual steps

[a] T. Neumann, W. Wenzel
Center for Functional Nanostructures, Karlsruhe Institute of Technology,
Wolfgang Gaede Str. 1a, Karlsruhe 76131, Germany
E mail: wolfgang.wenzel@kit.edu

[b] T. Neumann, D. Danilov, W. Wenzel
Institute of Nanotechnology, Karlsruhe Institute of Technology, Hermann
von Helmholtz Platz 1, Eggenstein Leopoldshafen 76344, Germany

[c] C. Lennartz
BASF SE, Modelling Organic Electronics, GVE/M B9, Ludwigshafen 67105,
Germany

help to ameliorate the problem, but the problem of relaxation on long time-scales remains.

Simulating morphologies with MD- or MC-based methods requires evaluation of the energy/forces, which requires typically evaluation of $O(N^2)$ energy terms for every simulation step, although this effort can be reduced for very large samples. To speed up the simulation and permit generation of larger samples, we investigate a novel scheme that aims to emulate the process of molecular beam epitaxy, where a few molecules at a time are deposited, while the majority of the sample changes little. Implementing this approach results in a modeling process the computational cost scales only linearly with the sample size. This scheme consists of two steps: in the first step, during the deposition of a new molecule, all previously deposited molecules remain fixed and create a static effective external potential. As the new molecule influences the energy landscape in a limited neighborhood once it has reached the film, the second optional step, permits relaxation of the molecules in this neighborhood. As only a few molecules are mobile in each of these steps, precomputation of the effective external potentials speeds up the simulation by orders of magnitude. However, as we show below, the approximations made in order to obtain this speedup must be carefully calibrated to generate morphologies on atomistic scale of sufficient quality to be subsequently used to extract experimentally relevant information on the system.

To investigate whether such morphologies can be created by the single molecule deposition scheme and to test the effect of the additional local relaxation on the quality of the samples, we applied the method to five different systems: argon, buckminsterfullerene (C_{60}), N,N-Di(naphthalene-1-yl)-N,N'-diphenyl-benzidine (α-NPD), tris(8-hydroxy-quinoline)aluminum(III) (Alq_3), and phenyl-C_{61}-butyric acid methyl ester (PCBM). We found that the deposition of amorphous samples for α-NPD, Alq_3, and PCBM generated amorphous morphologies with densities comparable to experimental values and to MD simulations. The application of local relaxation on these systems leads to higher densities but no significant change in the radial distribution function. In contrast, local relaxation has a significant impact for the deposition of Argon and C_{60}, resulting in crystalline structures. For Alq_3, we additionally investigated the impact of different simulation and force field parameters on the density. A postdeposition-relaxation of the whole sample using MC lead to the expansion of the system, indicating that the deposition yields conformations which are more denser than cooled liquids.

Computational Method

MC deposition protocol

As their invention in the 1950s, MC methods have been applied in many scientific areas including mathematics, physics, and economy.[14,15] In MC simulations, random changes are proposed to the last configuration in the Markov chain and an acceptance criterion is used to extend the chain commensurate with the underlying thermodynamic ensemble.

With the Metropolis acceptance criterion, moves that lead to energetically better configurations are always accepted, whereas moves leading to configurations with higher energy are accepted with a probability of the Boltzmann-factor.

We generate disordered morphologies using a deposition protocol that emulates vapor deposition of molecular films. The protocol consists of two steps: the first, mandatory step is deposition of a single molecule on a partially formed film using a basin hopping protocol. The second, optional step consists of selection of a neighborhood around the previously deposited molecule and its postdeposition relaxation via an annealing method.

The algorithm for the single molecule deposition step includes three nested blocks. In the outer block (Fig. 1a), the deposition of one new molecule to the existing film is performed. The loop consists of two main steps: deposition of the molecule and subsequent adjustments of the grid representations for electrostatic interactions (the details on the electrostatic grid representations are given in Effective potential for electrostatic interactions section). In the deposition step, a single molecule (Fig. 1b) starts from a random initial position above the surface of the film in the potential of the substrate, previously deposited molecules and a weak linear potential toward the surface, which is reduced to zero at a distance of one time, the size of the molecule above the film. In the simulations reported here, incoming molecules were placed 5 nm above the top surface of the film. The guiding potential reduces the time of random diffusion far above the film and prevents escape from the surface, when the molecule is still far from the surface and the intermolecular forces are small. Periodic boundary conditions are applied for the coordinates parallel to the surface.

On a very rugged potential energy surface, such as those induced by the roughness of the partially deposited film, simulations can be trapped for long times in metastable conformations. Such entrapment would result in films with much lower densities than observed experimentally. To reduce the trapping of the system in metastable conformations, use a basing hopping approach,[16–18] which comprises several simulated annealing simulations.[19] Each simulated annealing process starts at a high temperature T_S, where the molecule can easily traverse the energy barriers separating local minima. The temperature is lowered gradually during the simulation and the temperature T_n at step n varies geometrically with n as:

$$T_n \quad T_S \cdot c^n, \qquad c \quad \left(\frac{T_E}{T_S}\right)^{\frac{1}{N}} < 1 \tag{1}$$

where T_E is the end temperature and N is the total number of steps in simulated annealing run.

The temperatures used for simulated annealing need to be adapted to the problem at hand. For most simulations performed in this investigation, the initial temperature was set to 1000 K and cooled down to 300 K. The individual rigid body moves in the simulated-annealing simulation are the standard MC moves, consisting in equal fractions of rigid-body displacements, drawn from a Gaussian distribution with a standard
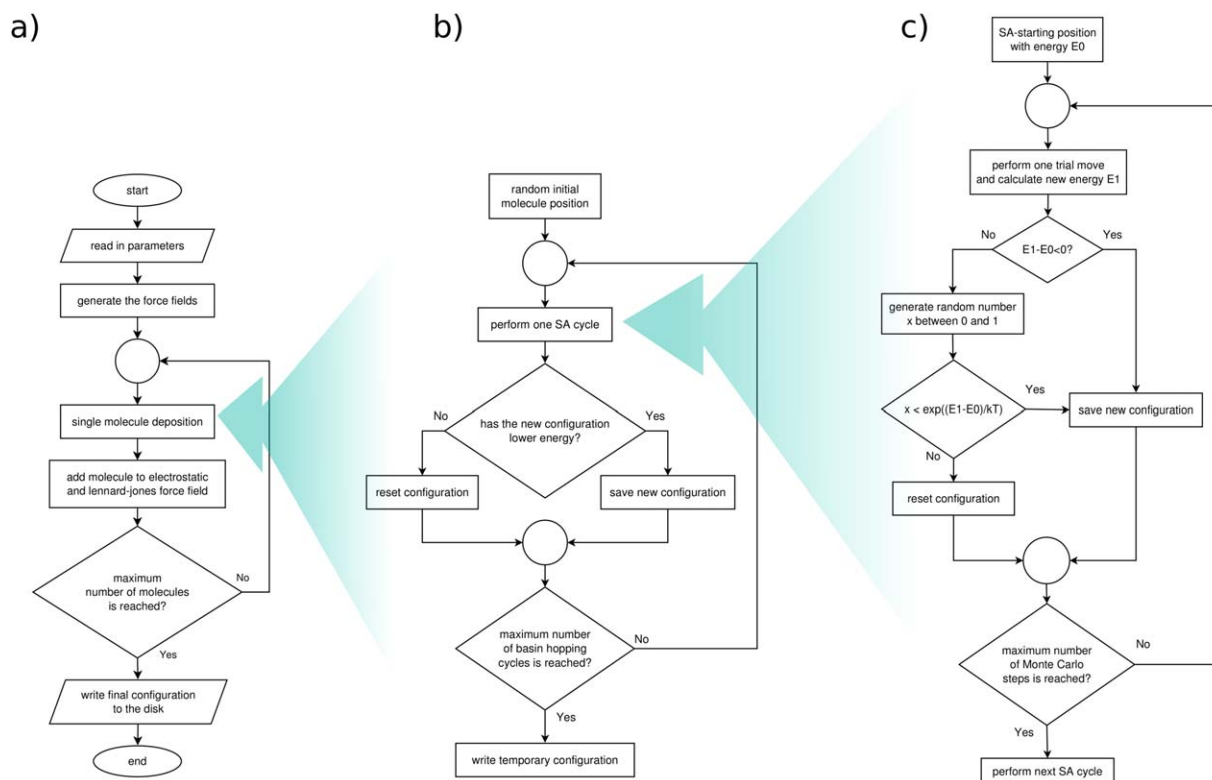
Figure 1. Workflow of the single molecule deposition protocol. (a) After reading in parameters and creating the effective external potentials, molecules are added one at a time to the structure. (b) The deposition of each molecule, starting at a random position above the structure, consists of several basin hopping cycles. If one cycle leads to an energetically favorable configuration, this configuration is starting point of the next basin hopping cycle. (c) Each basing hopping cycle consists of a series of *N* MC moves (random translations or rotations). Each move is accepted or rejected according to the Metropolis acceptance criterion. Throughout the cycle the temperature is decreased continuously to allow the molecule to cross barriers in the energy landscape in the beginning but end at a local minimum. [Color figure can be viewed in the online issue, which is available at wileyonlinelibrary.com.]

deviation of 0.1 nm, and rigid-body rotations around a random axis with an angle drawn from a Gaussian distribution with a standard deviation of $0.2\,\pi$. We found a Gaussian distribution to be preferable over a uniform random distribution: it allows for a limited number of larger moves throughout the simulation to cover a large phase space but also leads to a large fraction of small moves. Small moves are essential for a detailed and efficient sampling of the rough energy surface once the molecule approaches the surface. A good choice for the Gaussian parameters is essential for the efficiency of the simulations: small values lead to small changes in the system, which increases the number of MC steps necessary. Large moves lead to energetically unfavorable configurations that are likely to be rejected. This decreases the acceptance rate and with that increases the number of necessary MC steps. Deviations of this protocol and criteria for intermolecular moves are described below where needed. The standard deviation of the Gaussian distribution can be adjusted depending on the system under consideration. In the Results and Discussion section, we discuss the convergence of the results with respect to the number of MC steps per basin hopping cycle.

At the end of the annealing cycle, the energy of the conformation is compared with the energy of the conformation of the previous basin hopping cycle and will be accepted when the energy of the most recent conformation was lower than that of the previous cycle. Here, we performed $N\ 10$ basin-

hopping cycles. This enables the molecule to hop from one local minimum to another in the global energy landscape. The basin hopping approach[16–18] has been widely used as a straightforward, yet efficient energy optimization method for many problems,[18,20–22] including cluster optimization.[23–25] We would like to state at this point that the basing hopping approach is not equivalent to a standard MC simulation at zero temperature. The basing hopping is used to jump between different local minima. In each minima, an MC run is performed at a finite temperature well above $T\ 0\ K$ leading to configurations above the absolute optimum.

Interatomic potentials

The interaction between the molecules is described by non-bonded forces, here represented by electrostatic interaction and the Lennard-Jones potential as approximation of van der Waals interaction and Pauli repulsion. The electrostatic interaction energy of a molecule A in the field of a second molecule B is calculated as a sum of the products of each point charge with the electrostatic potential at the charge position

$$U_{\text{Coulomb}}\ \sum_{i}^{N_{\text{A}}} q_i\ \Phi\ (\vec{r}_i) \tag{2}$$

where the electrostatic potential $\Phi\ (\vec{r}_i)$ at position $\vec{r}_i$ reads

$$\Phi(\vec{r}_i) = \frac{1}{4\pi\epsilon\epsilon_0} \sum_{j}^{N_B} \frac{q_i}{r_{ij}} \qquad (3)$$

In eqs. (2) and (3), $r_{ij} = |\vec{r}_i - \vec{r}_j|$ is the distance between atoms i and j, N_A and N_B are the numbers of atoms in the molecules A and B, ε is the relative permittivity of the material, and ε_0 is the vacuum permittivity. At present, we use standard-nonpolarizable force fields in our calculations, but polarization can be included by using polarizable force fields. In order to efficiently account for polarization effects of the already deposited film, while preserving linear scaling, the electrostatic grid should then be generated not by performing the Coulomb sum in eq. (3), but using an efficient external solver of the Poisson Boltzmann equation, such as APBS (Adaptive Poisson-Boltzmann Solver). The partial charges can be computed, for example, by a best fit procedure from quantum mechanical calculations[26] in such a way that the set of the point partial charges q_i reproduces the true electrostatic potential on a defined surface around the molecule.

The van der Waals interaction and Pauli repulsion between two molecules is calculated using the Lennard-Jones potential

$$U_{LJ}(r) = \sum_{i}^{N_A} \sum_{j}^{N_B} 4\epsilon_{ij} \left(\left(\frac{\sigma_{ij}}{r_{ij}}\right)^{12} - 2\left(\frac{\sigma_{ij}}{r_{ij}}\right)^{6} \right) \qquad (4)$$

where r_{ij} is the distance between atoms i and j, N_A and N_B are the numbers of atoms in the molecules A and B, ε_{ij} is the potential well depth, and σ_{ij} is the radial parameter. The parameters for the interactions between atoms A and B are obtained from atomic parameters using standard mixing rules.

In contrast to the electrostatic interaction, the Lennard-Jones Potential is relatively short ranged. This allows us to introduce a cutoff for the Lennard-Jones potential and only consider energy contributions of close atoms.

The degrees of freedom were chosen in accordance with the material characteristics (see Results and Discussion section): Alq_3, C_{60} are treated as rigid bodies while for α-NPD and PCBM rotations around single bonds were considered. In general, the computational single-molecule deposition protocol is not limited to rigid molecules and intramolecular interactions can be taken into account.

Effective potential for electrostatic interactions

Evaluating energies by direct summation of particle–particle interaction induces an $O(N^2)$ step in the energy calculations, which dominates the computational effort. To reduce the simulation effort to $O(N)$, we implemented two measures: a cutoff in the short-ranged Lennard-Jones force field limits the number of atoms for the energy evaluation and yields a (more or less) constant contribution to the simulation time (particles within range are determined by domain decomposition). However, cutoffs for long-ranged electrostatic interactions often result in unphysical results. We, therefore, subdivide the system into two components: one component can change during the simulation, whereas the other is kept fixed and yields a

static electrostatic potential. In step 1 of the deposition simulation, the first component contains only the new molecule being deposited, in step 2, it is enlarged to include the relaxation neighborhood. We calculate the (static) electrostatic potential of the fixed molecules on a mesh and use linear interpolation to calculate the potential for all points in space.

After deposition of a new molecule the electrostatic potential on the grid points need to be updated. As the Coulomb potential is additive, updating the mesh is $O(1)$ for each new molecule, but scales with the number of mesh points. The time gain using the grid-method depends on the number of molecules being deposited and the mesh-spacing of the grid. The error in energy induced by interpolation depends on the mesh-spacing as well. To determine this error, we simulated the deposition of a dummy-charge on a surface consisting of 100 Alq_3 molecules using one SA-cycle (Simulated-Annealing-cycle) with 10,000 MC steps and a grid spacing of 0.05 nm.

Retracing the resulting trajectory, we calculated electrostatic energy after every MC step for both different mesh sizes (grid spacings) and exact summation of the particle–particle interactions. As for the acceptance of a move only energy differences ΔE are taken into account, we calculated ΔE for each step and compared values for different grid spacings with the values obtained without Coulomb-mesh. We then calculate the relative error $\Delta\Delta E$ in relation to the electrostatic energy, $\Delta\Delta E_{Coulomb}$, and the total energy, $\Delta\Delta E_{tot}$, according to

$$\Delta\Delta E_{Coulomb/tot} = \frac{\Delta E_{total}^{grid} - \Delta E_{tot}^{nogrid}}{\Delta E_{coulomb/tot}} - \frac{\Delta E_{coulomb}^{grid} - \Delta E_{coulomb}^{nogrid}}{\Delta E_{coulomb/tot}^{nogrid}}$$

$$(5)$$

The dependence of the relative error (averaged over all 10,000 MC steps) on the grid spacing is shown in Figure 2. Although the error increases with the mesh spacing, we find that the error is sufficiently small for grid spacings below 0.1 nm. The use of an electrostatics grid incurs a computational effort to update the effective external potential after the deposition, which is more than compensated by a time gain in the energy evaluation of each MC step. By recording simulation times for the deposition of 30 Alq_3 molecules containing 52 atoms each with typical parameters (10 simulated annealing cycles with 20,000 MC steps per cycle) for both grid method with a grid-spacing of 0.05 nm and direct evaluation of the pair interaction, we find an overall speedup of at least one order of magnitude after deposition of the first 10 molecules. As the numbers of the calculation steps needed for the interpolation between the values on the grid points and of the calculation steps for updating the grid after each deposition are independent on the number of molecules already in the system, the use of an electrostatics grid together with the cutoff in the Lennard-Jones potential leads to a constant deposition time.

Local relaxation step

During the deposition of a single molecule, molecules deposited in prior cycles in the film are kept fixed. This approximation
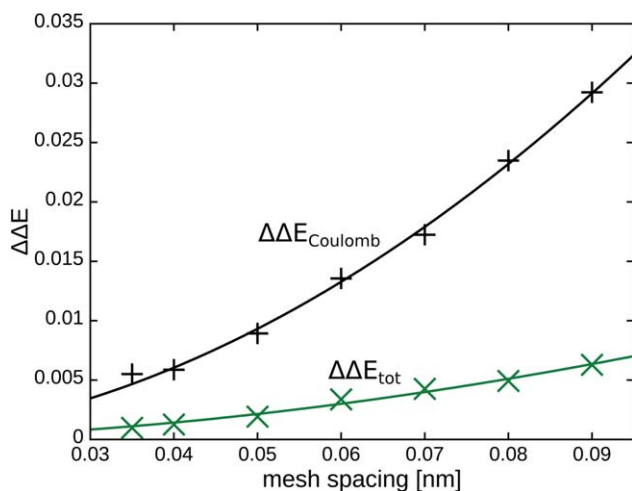
Figure 2. Error in the Coulomb energy caused by the linear interpolation between grid points in relation to electrostatics (black) and in relation to total energy (green). The error was measured by retracing a trajectory con sisting of 10,000 MC steps for different mesh spacings and calculating the difference between change of energy with grid method and the change of energy obtained by direct summation of particle particle interactions. [Color figure can be viewed in the online issue, which is available at wileyonlinelibrary.com.]

allows rapid morphology generation but once the new molecule reaches the film it will change the potential of previously deposited molecules. This problem is most severe for crystalline materials: As Figure 3 illustrates, the energy landscape of a crystal surface of pentacene leads to an optimal orientation of an additional molecule, which differs by $\sim 60^{\circ}$ (right) in comparison to the bulk crystal structure (left). Because the energy of this conformation is better than the corresponding crystal position, relaxation to the crystal position can only take place after several additional layers have been deposited. To overcome this problem, we introduce the second step in the deposition protocol: after the deposition of a molecule, this molecule and a selected number of neighbors in the previously deposited film are allowed to relax during additional simulated annealing cycles. To this end, we select all molecules within a cutoff distance r_0 from the new molecule, remove them from the effec-

tive external potential and evaluate their interactions explicitly. Because the vast majority of the molecules in a large sample still remain inert, the numerical procedure retains its $O(1)$ character, albeit with a high prefactor. However, the number of MC moves per additional simulated annealing cycles should grow with the number of molecules involved into the local relaxation to allow for equilibration.

Results and Discussion

In this section, we discuss the results of morphology simulations for five different systems of increasing complexity. First, we focus on comparatively simple systems, which should form phases with long-range order, which is a particular challenge for a single molecule deposition method: argon, buckminsterfullerene (C_{60}). We then investigate some widely used materials in organic electronics N,N-Di(naphthalene-1-yl)-N,N'-diphenyl-benzidine (α-NPD), mer-tris(8-hydroxy-quinoline)aluminum(III) (Alq_3) and PCBM.

Argon

At low temperature, the noble gas Argon forms a crystal.[28] Because interactions between atoms are well described by the Lennard-Jones potential, we have studied Argon as simplest test system in order to investigate the effect of the local relaxation step (Local relaxation step section) on the deposited morphology. The Lennard-Jones parameters σ 0.34 nm and ε 0.238 kcal/mol are adopted from Ref. [29]. In three simulations, one without local relaxation, and two including local relaxation with cutoff radii for neighborhoods selection of r_0 0.39 nm and r_0 0.77 nm, respectively, we deposited approximately 6000 atoms into a box of size 8×8 nm^2 in each simulation using 10 basin hopping steps with N_{MC} 2.5 $\times 10^4$ MC steps each. The simulated annealing simulation starts with the temperature 20,000 K and ends at 10 K, which lies below the melting point 83.78 K.[30] The cutoff distances of r_0 0.39 nm and r_0 0.77 nm correspond approximately to one and two times the nearest neighbor distance in the argon crystal.[28]
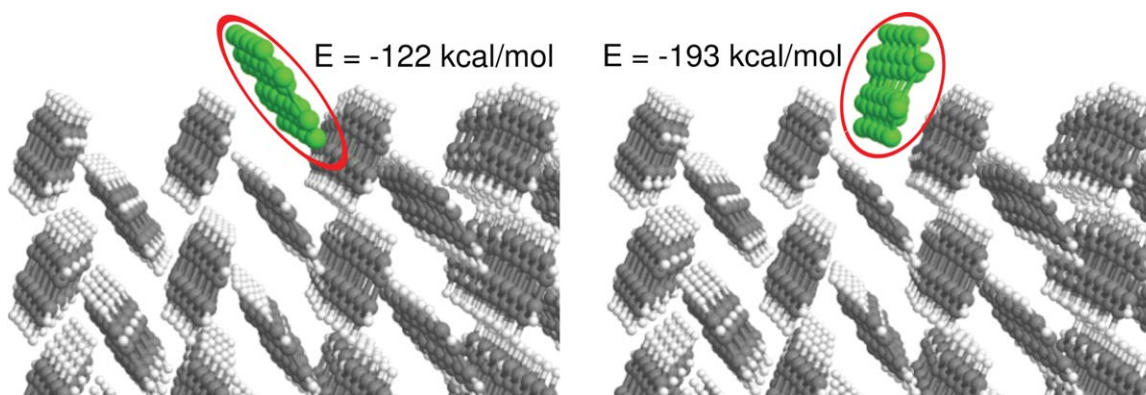
Figure 3. (a) Orientation of a pentacene molecule in the bulk of the pentacene crystal,[27] (b) orientation of a pentacene molecule at the end of the single molecule deposition. The configuration found by the single molecule deposition is energetically favorable. |However, #this configuration differs from the configuration of a molecule in the bulk of the pentacene crystal which becomes energetically favorable only if the molecule is surrounded by other penta cene molecules. [Color figure can be viewed in the online issue, which is available at wileyonlinelibrary.com.]

Due to the attractive surface force field at the bottom of the box, the first three layers readily form a hexagonal closest packed structure. To be able to better compare simulations of deposition with and without local relaxation, these layers were not taken into account in the evaluation of the resulting morphologies. Figure 4 shows the radial distribution functions $g(r)$ of the three structures as well as $g(r)$ of a perfect fcc-crystal in 111-direction. Although deposition without relaxation results in morphologies with no long-range order, simulations with additional local relaxation lead to strong peaks in $g(r)$, an effect which increases with increasing cutoff-radius for neighborhood selection.

To evaluate the effect of the final temperature of the Simulated Annealing-cycles on the structure, we generated two additional morphologies using local relaxation with r_0 0.77 nm at temperatures 100 and 150 K and computed the radial distribution functions. The radial distribution function $g(r)$ for both T_f 10 K and T_f 100 K have strong peaks, whereas the structure generated with T_f 150 K is very disordered. This is commensurate with the fact that the melting point of argon is T_{melt} 83.78 K, because acceptance criterion of the basis hopping step induces a nonequilibrium effect, which corresponds to an effective lower temperature in the simulation.

Buckminster-Fullerene C_{60}

Next, we examine a system of C_{60} Buckminsterfullerene molecules, which is still described by Lennard-Jones interactions, but has a more complex molecular structure. This molecule was first observed by Robert Curl, Harold Kroto, and Richard Smalley in 1985.[31] Like Argon, C_{60} molecules form fcc-crystals with a length of the unit cell of 1.4 nm.[32] With a sublimation temperature of $T_{subl} \approx 875$ K, C_{60} is a good candidate for testing the deposition protocol.[33] As C_{60} molecules consist only of carbon atoms which carry no appreciable partial charges, only Lennard-Jones interactions are considered (σ 0.389 nm and ε 0.06595 kcal/mol).[34]

As a first test, we deposited C_{60} molecules into a box of $8 \times 8 \times 11.3$ nm^3 using 10 Simulated Annealing-cycles with 2×10^4 steps each, a Lennard-Jones cutoff of 1.5 nm and a final temperature of 10 K without local relaxation. To evaluate long-ranged ordering, we applied an Ackland analysis using the program *ovito*.[35,36] The results are displayed in Figure 4b. The first five layers form a fcc-crystal in the 111-direction perpendicular to the surface, but this ordering is lost above those layers and presumably an effect of the surface force field. This can also be seen in densities: the density of the lower five layers is ρ 1.57 g/cm^3, whereas we measured a density of ρ 1.45 g/cm^3 in the upper part of the structure.

Next, we generated two additional structures using simulations with local relaxation with r_0 1.07 nm and r_0 1.6 nm, respectively, 10 SA-cycles and an additional 1000 steps per molecule and cycle in the relaxation step. To eliminate the effect of the surface potential on the evaluation, the lower five layers were not taken into account for further evaluation of the results. Figure 4b shows the radial distribution functions $g(r)$ in comparison with $g(r)$ of a perfect fcc-crystal. With the C_{60} molecules,

a)

b)
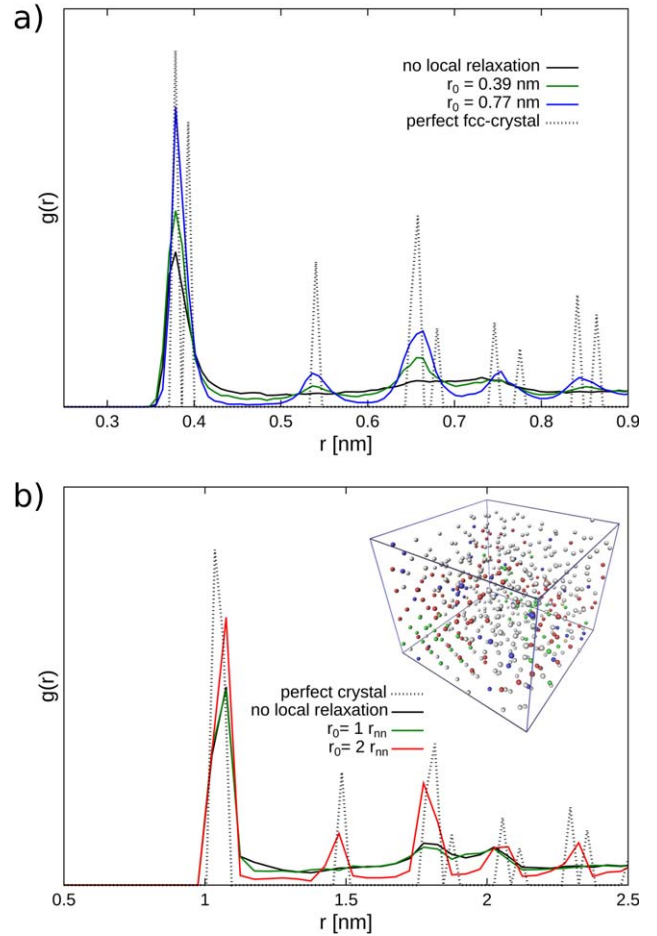
Figure 4. (a) Radial distribution functions $g(r)$ of Argon structures created without local relaxation (black), using local relaxation with r_0 0.39 nm (green) and r_0 0.77 nm (blue) and $g(r)$ of a perfect fcc crystal (dashed). Whereas the structure without relaxation shows no long range order, local relaxation with r_0 0.77 nm produces an ordered structure with peaks near the positions of those of the perfect crystal. (b) Radial distribution functions of C_{60} structures generated with local relaxation using r_0 1.07 nm (green) and r_0 1.6 nm (red), of the structure generated without local relaxation (black) and $g(r)$ of a perfect crystal. The structures generated without local relaxation and with r_0 1.07 nm correspond to disordered structures. $g(r)$ of the structure generated with r_0 1.6 nm shows long range order. Inset: Ackland analysis of the centers of geometry of C_{60} structures generated at T 10 K using local relaxation with r_0 1.6 nm. Green coloring indicates fcc structures, the red parts at the edges hexagonal closest packing.

local relaxation has the same effect as with argon atoms: choosing r_0 large enough, we were able to deposit the molecules into a crystalline phase. This is confirmed by the Ackland analysis with the structure generated with r_0 1.6 nm. In the inset of Figure 4b, the inner layers are clearly identified as a fcc-structure. The density of the structure generated with r_0 1.6 nm is ρ 1.46 g/cm^3, that is, somewhat lower than the density of the first five crystalline layers of the structure generated without local relaxation, which may be due to local defects in the structure.

Alq$_3$

Mer-Tris(8-hydroxyquinolinato)aluminium (Alq$_3$), has been studied as electron-transporting and light emitting material since

Tang and VanSlyke reported[37] its use in OLED for the first time. Recently, possibilities to use Alq_3 as a buffer layer in organic solar cells have been investigated. As a buffer layer, Alq_3 is believed to obstruct the permeation of oxygen and moisture into the photoactive layer, thus increasing the stability and lifetime of the organic solar cells.[38] A layered organic solar cell with Alq_3/Au as cathode showed an efficiency enhancement by a factor of 60, from 0.01 to 0.60%, compared to a cell without Alq_3.[39] The crystal structure for the mer-isomer of Alq_3 is reported in Ref. [39] and has a density of 1.37 g/cm^3. The reported experimental values for the density of the amorphous phase of Alq_3 vary in a range from 1.3[40] to 1.5 g/cm^3.[41] The large variation in the density of the amorphous films indicates a strong dependency on details of the sample preparation method.

For Alq_3, partial charges (see Interatomic potentials section) were obtained from an electrostatic potential fit[26] for a single molecule. The electronic structure was computed with density functional theory as implemented in TURBOMOLE[42] using a def2-TZVP basis set[43] and B3LYP functional[44] in the molecular geometry from the crystal structure. Mol2 files of the geometry including partial charges of Alq3 and the following molecules are printed in the supporting information. For Lennard-Jones interactions, we used parameters from the all-atom Dreiding force field[45] and from the OPLS (Optimized Potential for Liquid Simulations) force field.[46] To compare the impact of different Lennard-Jones-parameters on the deposition, we calculated the densities of Alq_3 structures generated with Dreiding and OPLS force field for different numbers of MC moves per basin hopping cycle. The results are shown in Figure 5. We find that the OPLS force field gives higher densities (1.22 g/cm^3) than the Dreiding force field (1.15 g/cm^3). For both force fields, densities stay approximately the same when more than 20,000 MC steps are used per molecule deposition.

In order to get a better estimate of the quality of the structures generated using the single molecule deposition, we relaxed structures deposited without local relaxation and with local relaxation using r_0 1.5 nm at constant temperature (300 K) using 2×10^6 MC steps. We recorded the density throughout the simulation. The results are displayed in the inlay of Figure 6a. The densities were decreasing, not increasing, for both samples throughout the simulation. Thus, the single molecule deposition is producing closer packed structures than MC methods applied to the whole sample. This indicated that the deposition protocol used here can generate samples with very high densities for the force field used.

To compare structures obtained with the single molecule deposition protocol, with those obtained from MD, the most widely used method today, we simulated 300 Alq_3 molecules for 4.2 ns using the GROMACS MD package[47] with general amber force field (GAFF) dihedral force fields, but, as in the deposited structures, Dreiding LJ (Lennard-Jones) and the partial charges as described above. The initial configuration was generated by the single molecule deposition using only 500 steps per simulated annealing cycle. This structure was far from being converged and contained many low-density pock-
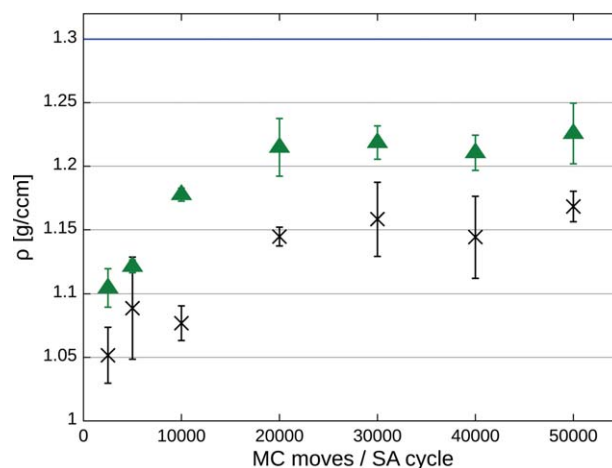
Figure 5. Alq_3 density versus number of MC steps per basing hopping cycle for OPLS (green) and Dreiding (black) force field. More than 20,000 steps yield a constant density which is lower that the literature value of 1.3 g/cm^3. [Color figure can be viewed in the online issue, which is available at wileyonlinelibrary.com.]

ets. We used a Berendsen barostat[48] with p 1 atm, T 300 K, and a time step of Δt 0.5 fs. The radial distribution functions of the structures generated with the deposition protocol with and without local relaxation and with different dielectric constants is compared to the radial distribution of the MD (structure in Fig. 6a).

The reason for the somewhat tighter packing in the MD simulation stems from the presence of intramolecular degrees of freedom that were neglected in the single molecule deposition protocol. We have analyzed the change of the angles α, β, and γ between the three flaps of the Alq_3 molecules in the MD run as bending of the side groups allows the molecules to come closer to each other. For a molecular geometry optimized at the DFT (Density Functional Theory) level, these angles are: α_0 93.56°, β_0 167.16°, γ_0 94.50°. The mean value of the same angles for all molecules extracted from the MD deviate strongly from these values and show a wide distribution: α 124.67° $\pm$ 17.48°, β 124.00° $\pm$ 22.72° γ 102.35° $\pm$ 16.20° The general amber force field (GAFF) force field appears to permit very strong distortion in all angles which permits closer local packing. We note that the MD simulations take considerably longer: MD, using 16 cores on standard Intel Nehalem 2.8-Ghz processors produces trajectories with a length of only 0.11 ns per day for a system containing 350 molecules, whereas the MC-based deposition protocol produces morphologies consisting of about 300 molecules per day using only a single core. In future work, it is nevertheless necessary to incorporate the more complex intramolecular degrees of freedom (bending, bon-stretching) into the single molecule deposition protocol. Until this method is available morphologies generated with the single molecule deposition protocol should be postrelaxed in short MD simulations, which will not change the relative orientation of molecules but locally relax the structure.

As Alq_3 is a prototypical and widely studied example for disordered organic materials of practical relevance, it is
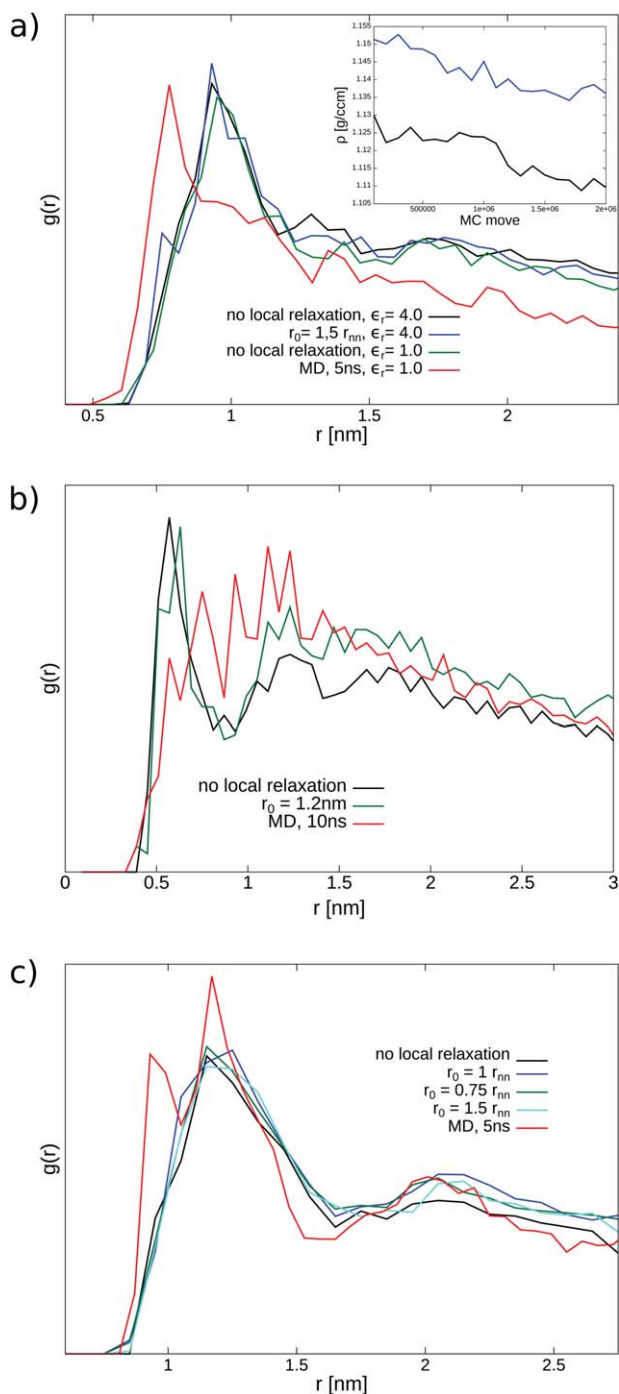
Figure 6. (a) Radial distribution functions of Alq$_3$ structures generated with singe molecule deposition with and without local relaxation and two different dielectric constants (consisting of approximately 500 molecules each) and with a 5 ns MD run of 350 molecules. The deposited molecules were treated as rigid bodies, whereas the molecules in the MD simulations had internal degrees of freedom as parameterized by the general amber force field (GAFF) force field. (b) Radial distribution functions of α NPD structures generated with MD (10 ns, 295 molecules) and structures deposited with our protocol, generated with and without local relaxation. The local relaxation steps leads to appearance of a secondary peak in g(r). (c) Radial distribution functions of PCBM structures, deposited with our protocol and generated with MD (5 ns). The nearest neighbor peak is at the same distance for both methods with little impact of local relaxation on the morphologies.

interesting to analyze the computational cost of our protocol for this example. There is a competition between the computational efficiency and the accuracy of the relaxation-approximation on the arrangement of the molecules. Whether it is necessary to include the local relaxation can be examined by comparing the results of small or middle size test simulation, with and without the local relaxation. If there is no significant effect of the local relaxation step on the characteristic properties of the structure, then the local relaxation can be switched off in the production large size samples. In order to estimate the additional costs induced by the local relaxation, we recorded the deposition times for a sample of 60 molecules using different cutoff radii. For the cutoff radius r_0 1.1 nm using 2000 moves per molecule results in an acceptable doubling of the computational effort.

α-NPD

Another widely used material in production of OLEDs is α-NPD (N,N-Di(naphthalene-1-yl)-N,N'-diphenyl-benzidine). Because α-NPD has internal degrees of freedom (seven dihedral angles that are not part of aromatic rings), we increased the number of MC steps to 40,000 for each deposition cycle. The end temperature of the simulated annealing was 300 K. We generated models with and without local relaxation and additionally performed MD simulations with 290 α-NPD molecules (Δt 0.5 fs, 1 atm, 300 K) for 10 ns starting from a structure obtained by a single-molecule deposition process with very short cycles, creating a morphology far from converged state. The Lennard-Jones (LJ) parameters were taken from the OPLS force field, the partial charges taken from quantum chemical calculations using TURBOMOLE with a def-2-TZVP basis set and the B3LYP functional by means of electrostatic potential fit.

The radial distribution functions of the deposited structures generated with and without local relaxation with the radial distribution function of a structure obtained by MD (10 ns) using the same force field parameters are shown in Figure 6b. The nearest neighbor peaks of the deposited structure are stronger than the peak of the MD structure, indicating an insufficient simulation time for the MD run. The MD run generated a trajectory of 0.387 ns/day resulting in a total simulation time of approximately 1 month. The local relaxation leads to a slightly stronger second peak in the radial distribution function.

PCBM

PCBM (the fullerene derivative [6,6]-phenyl-C$_{61}$-butyric acid methyl ester) is used in organic photovoltaic and forms crystalline structures. We deposited PCBM with and without local relaxation using 50,000 MC steps/cycle for the deposition and 5000 MC steps/molecule and cycle for the local relaxation. The Lennard-Jones parameters for the carbon atoms in the fullerene were taken from the same force field used for the C$_{60}$-buckyballs above,[34] the parameters for the side chain atoms were again taken from the OPLS force field. The partial charges were obtained by the same TURBOMOLE calculations

as with the other molecules. We compared the resulting structures with a structure generated by a 10-ns MD run (0.67 ns/day using 16 cores with 2.8 GHz each) with the same settings as used for α-NPD.

The radial distribution functions for the different single-molecule deposition runs (with and without local relaxation) as well as the MD run are displayed in Figure 6c. The choice of the local relaxation radius seems to have no visible effect on the radial distribution functions. The nearest neighbor peak is at roughly the same position for both the MD simulation and the structures generated by single-molecule deposition.

Summary and Conclusions

Quantitative multiscale modeling of organic semiconductor devices on the basis of their molecular constituents requires efficient computational methods for the simulation of morphologies of small molecule thin films on atomistic scale. The morphology of the organic film has a tremendous impact on their electronic structure and transport properties, as local disorder in energy is one key property of these systems. Models for large morphologies consisting of many thousands of molecules are necessary in order to obtain sufficient statistics for the characteristic properties (e.g., in site energies) of the material. Here, we have developed and applied a novel, linear-scaling protocol to generate morphologies using readily accessible computational resources. This computational protocol mimics the physical process of vapor deposition as used in production of OLEDs. We applied the method to five different systems: argon, buckminsterfullerene (C_{60}) as examples for systems with long range order, N,N-Di(naphthalene-1-yl)-N,N'-diphenyl-benzidine (α-NPD), mer-tris(8-hydroxy-quinoline)aluminum(III) (Alq_3), and PCBM as examples for typical disordered organic thin film materials. We found that the deposition of amorphous samples for α-NPD, Alq_3, and PCBM generated amorphous morphologies that compare well with experimental densities and MD simulations. The application of local relaxation on these systems leads to higher densities but no significant change in the radial distribution function. It was interesting to note that postrelaxation of the amorphous samples with either MC or MD tended to decrease rather than increase their packing density. This observation could be explained by recent experimental evidence regarding vapor deposition protocols for molecular structures: it appears that configurations of amorphous structures generated by vapor deposition are more stable than the configurations obtained by cooling liquids,[49] because molecules deposited on a surface can explore a much larger conformation space than a particle supercritical solid phase. In contrast to the amorphous systems local relaxation showed a significant impact for the deposition of Argon and C_{60}, resulting in more ordered structures, but the protocol as a whole is well suited to model morphologies with long-range order. Future work needs to concentrate on improved treatment of intramolecular degrees of freedom and the development of efficient protocols to generate accurate force fields for organic molecules that are not well represented by standard force

fields. In addition, the protocol is easy to adapt to model organic–organic and organic–inorganic interfaces provided that suitable force fields are available. It can also be applied to treat doped organic layers and guest–host systems, which are of significant importance in applications in organic electronics.

[1] S. R. Forrest, *Nature* **2004**, *428*, 911.
[2] A. P. Kulkarni, C. J. Tonzola, A. Babel, S. A. Jenekhe, *Chem. Mater.* **2004**, *16*, 4556.
[3] A. Pron, P. Gawrys, M. Zagorska, D. Djurado, R. Demadrille, *Chem. Soc. Rev.* **2010**, *39*, 2577.
[4] J. Cornil, D. Beljonne, J. P. Calbert, J. L. Brédas, *Adv. Mater.* **2001**, *13*, 1053.
[5] V. Coropceanu, J. Cornil, D. A. da Silva Filho, Y. Olivier, R. Silbey, J. L. Brédas, *Chem. Rev.* **2007**, *107*, 926.
[6] N. Karl, K. H. Kraft, J. Marktanner, M. Munch, F. Schatz, R. Stehle, H. M. Uhde, *Fast Electronic Transport in Organic Molecular Solids?* 4th ed.; AVS: Baltimore, MA, **1999**; pp. 2318 2328.
[7] M. Flämmich, J. Frischeisen, D. S. Setz, D. Michaelis, B. C. Krummacher, T. D. Schmidt, W. Brütting, N. Danz, *Org. Electron.* **2011**, *12*, 1663.
[8] D. Yokoyama, *J. Mater. Chem.* **2011**, *21*, 19187.
[9] W. Kob, H. C. Andersen, *Phys. Rev. E* **1995**, *51*, 4626.
[10] S. Sastry, P. G. Debenedetti, F. H. Stillinger, *Nature* **1998**, *393*, 554.
[11] A. Lukyanov, C. Lennartz, D. Andrienko, *Phys. Stat. Sol.* (a) **2009**, *206*, 2737.
[12] F. May, M. Al Helwi, B. Baumeier, W. Kowalsky, E. Fuchs, C. Lennartz, D. Andrienko, *J. Am. Chem. Soc.* **2012**, *134*, 13818.
[13] J. J. Kwiatkowski, J. Nelson, H. Li, J. L. Bredas, W. Wenzel, C. Lennartz, *Phys. Chem. Chem. Phys.* **2008**, *10*, 1852.
[14] R. E. Caflisch, *Acta Numer.* **1998**, *7*, 1.
[15] P. Glasserman, *Monte Carlo Methods in Financial Engineering*; Springer, New York, **2004**.
[16] Z. Li, H. A. Scheraga, *Proc. Natl. Acad. Sci. USA* **1987**, *84*, 6611.
[17] D. J. Wales, J. P. K. Doye, *J. Phys. Chem. A* **1997**, *101*, 5111.
[18] D. J. Wales, H. A. Scheraga, *Science* **1999**, *285*, 1368.
[19] S. Kirkpatrick, C. D. Gelatt, M. P. Vecchi, *Science* **1983**, *220*, 671.
[20] A. Verma, A. Schug, K. H. Lee, W. Wenzel, *J. Chem. Phys.* **2006**, *124*, 044515.
[21] E. Zaccarelli, *J. Phys. Condens. Matter* **2007**, *19*, 323101.
[22] S. M. Woodley, R. Catlow, *Nat. Mater.* **2008**, *7*, 937.
[23] D. J. Wales, M. P. Hodges, *Chem. Phys. Lett.* **1998**, *286*, 65.
[24] F. Baletto, R. Ferrando, *Rev. Mod. Phys.* **2005**, *77*, 371.
[25] R. Ferrando, J. Jellinek, R. L. Johnston, *Chem. Rev.* **2008**, *108*, 845.
[26] U. C. Singh, P. A. Kollman, *J. Comput. Chem.* **1984**, *5*, 129.

[27] Campbell, R. B., Robertson, J. M., and Trotter, J. (**1961**) The crystal and molecular structure of pentacene, *Acta Crystallographica 14*, 705 711.

[28] H. Kanzaki, *J. Phys. Chem. Solids* **1957**, *2*, 24.

[29] W. T. Ashurst, W. G. Hoover, *Phys. Rev. Lett.* **1973**, *31*, 206.

[30] F. Datchi, P. Loubeyre, R. LeToullec, *Phys. Rev. B* **2000**, *61*, 6535.

[31] H. W. Kroto, J. R. Heath, S. C. O'Brien, R. F. Curl, R. E. Smalley, *Nature* **1985**, *318*, 162.

[32] S. Liu, Y. J. Lu, M. M. Kappes, J. A. Ibers, *Science* **1991**, *254*, 408.

[33] R. Loutfy, E. Wexler, Perspectives of Fullerene Nanotechnology, Springer Netherlands, 2002, 275.

[34] L. Girifalco, M. Hodak, R. Lee, *Phys. Rev. B* **2000**, *62*, 13104.

[35] G. J. Ackland, A. P. Jones, *Phys. Rev. B* **2006**, *73*, 054104.

[36] A. Stukowski, *Model. Simul. Mater. Sci. Eng.* **2010**, *18*, 015012.

[37] C. W. Tang, S. A. VanSlyke, *Appl. Phys. Lett.* **1987**, *51*, 913.

[38] Q. L. Song, F. Y. Li, H. Yang, H. R. Wu, X. Z. Wang, W. Zhou, J. M. Zhao, X. M. Ding, C. H. Huang, X. Y. Hou, *Chem. Phys. Lett.* **2005**, *416*, 42.

[39] P. Vivo, J. Jukola, M. Ojala, V. Chukharev, H. Lemmetyinen, *Sol. Energy Mater. Sol. Cells* **2008**, *92*, 1416.

[40] G. G. Malliaras, Y. Shen, D. H. Dunlap, H. Murata, Z. H. Kafafi, *Appl. Phys. Lett.* **2001**, *79*, 2582.

[41] C. H. M. Marée, R. A. Weller, L. C. Feldman, K. Pakbaz, H. W. H. Lee, *J. Appl. Phys.* **1998**, *84*, 4013.

[42] R. Ahlrichs, M. Bär, M. Häser, H. Horn, C. Kölmel, *Chem. Phys. Lett.* **1989**, *162*, 165.

[43] F. Weigend, R. Ahlrichs, R, *Phys. Chem. Chem. Phys.* **2005**, *7*, 3297.

[44] A. D. Becke, *J. Chem. Phys.* **1993**, *98*, 5648.

[45] S. L. Mayo, B. D. Olafson, W. A. Goddard, *J. Phys. Chem.* **1990**, *94*, 8897.

[46] W. Damm, A. Frontera, J. Tirado Rives, W. L. Jorgensen, *J. Comput. Chem.* **1997**, *18*, 1955.

[47] B. Hess, C. Kutzner, D. van der Spoel, E. Lindahl, *J. Chem. Theory Comput.* **2008**, *4*, 435.

[48] H. J. C. Berendsen, J. P. M. Postma, W. F. van Gunsteren, A. DiNola, J. R. Haak, *J. Chem. Phys.* **1984**, *81*, 3684.

[49] S. Singh, M. D. Ediger, J. J. de Pablo, *Nat. Mater.* **2013**, *12*, 139.